

Near-Infrared Spectrophotometry of Phobos and Deimos

A. S. Rivkin^{1,2} and R. H. Brown²

Lunar and Planetary Laboratory, 1629 E. University Boulevard, Tucson, Arizona 85721

D. E. Trilling²

Department of Physics and Astronomy, University of Pennsylvania, David Rittenhouse Laboratory, 209 S. 33rd Street, Philadelphia, Pennsylvania 19104

J. F. Bell III²

Astronomy Department, Cornell University, 402 Space Sciences Building, Ithaca, New York 14853-6801

and

J. H. Plassmann¹

Lunar and Planetary Laboratory, 1629 E. University Boulevard, Tucson, Arizona 85721

Received September 25, 2000; revised August 31, 2001

We have observed the leading and trailing hemispheres of Phobos from 1.65 to 3.5 μm and Deimos from 1.65 to 3.12 μm near opposition. We find the trailing hemisphere of Phobos to be brighter than its leading hemisphere by 0.24 ± 0.06 magnitude at 1.65 μm and brighter than Deimos by 0.98 ± 0.07 magnitude at 1.65 μm . We see no difference larger than observational uncertainties in spectral slope between the leading and trailing hemispheres when the spectra are normalized to 1.65 μm . We find no 3- μm absorption feature due to hydrated minerals on either hemisphere to a level of $\sim 5\text{--}10\%$ on Phobos and $\sim 20\%$ on Deimos. When the infrared data are joined to visible and near-IR data obtained by previous workers, our data suggest the leading (Stickney-dominated) side of Phobos is best matched by T-class asteroids. The spectral slope of the trailing side of Phobos and leading side of Deimos are bracketed by the D-class asteroids. The best laboratory spectral matches to these parts of Phobos are mature lunar soils and heated carbonaceous chondrites. The lack of 3- μm absorption features on either side of Phobos argues against the presence of a large interior reservoir of water ice according to current models of Phobos' interior (F. P. Fanale and J. R. Salvail 1989, *Geophys. Res. Lett.* 16, 287–290; *Icarus* 88, 380–395). © 2002 Elsevier Science (USA)

Key Words: satellites of Mars; asteroid composition; infrared observations; spectrophotometry.

1. INTRODUCTION AND PREVIOUS WORK

Phobos and Deimos have long served as stand-ins for asteroids, and insights into their origin and composition are applied to these bodies (Veveřka and Thomas 1979). Spectral results from Mariner 9 and Viking lander cameras indicated that the satellites were best matched by carbonaceous chondrites (Pang *et al.* 1978, Pollack *et al.* 1978), although in later work Grundy and Fink (1992) and Murchie and Erard (1996) found much steeper spectral slopes for these bodies that were inconsistent with carbonaceous chondrites.

Using data from the VSK (visible imager) multichannel camera on the Phobos 2 spacecraft, Avanesov *et al.* (1991) found that Phobos had an unexpectedly low density ($1.9 \pm 0.1 \text{ g/cm}^3$). At that time, it was not thought that small bodies could support the high porosity implied by this density, and interpretations favored internal ice and a mineralogy like the lowest density meteorites, the CI/CM carbonaceous chondrites. This interpretation was supported by the spectral data available at the time. Because the CI/CM meteorites contain abundant hydrated minerals, and because internal ice was inferred, the satellites gained prominence as a possible source of fuel and materials needed for life support and as a staging area for human exploration of Mars. More recent density results from Smith *et al.* (1995) based on distant spacecraft encounters suggest even lower densities, with Phobos at 1.53 ± 0.1 and Deimos at $1.34 \pm 0.83 \text{ g/cm}^3$. The NEAR encounter with 253 Mathilde showed that asteroid to have an unexpectedly low density of $1.3 \pm 0.3 \text{ g/cm}^3$ (Veveřka *et al.* 1997), while Rivkin *et al.* (1997) found no evidence of hydrated minerals on Mathilde. Because numerous

¹ Now at Massachusetts Institute of Technology, 77 Massachusetts Avenue, Cambridge, MA 02139.

² Guest Observer at the Infrared Telescope Facility, operated by NASA and the University of Hawaii.

asteroids *do* show evidence of hydrated minerals (Lebofsky 1980, Feierberg *et al.* 1985, Lebofsky *et al.* 1990, Jones *et al.* 1990, Rivkin *et al.* 1995, 2000), we know that hydrated minerals can survive on asteroidal surfaces and that the lack of an absorption feature on 253 Mathilde is probably not a result of regolith processes but rather is a true reflection of its hydration state. This makes an interior reservoir of ice unlikely on Mathilde and precludes an association with the hydrated carbonaceous chondrites, implying high porosity as the explanation for Mathilde's low density. The finding that high porosities are possible on large asteroids implies that Phobos and Deimos could have large porosities as well.

The ISM infrared imaging spectrometer on board Phobos 2 provided the first infrared spectra of Phobos and the first evidence that Phobos lacked a deep hydration feature (Bibring *et al.* 1989). Murchie *et al.* (1991), using an early calibration for the VSK and KRFM (visible and UV spectrometer on Phobos 2) data, divided the surface of Phobos into four distinct spectral units: red, reddish gray, blue, and bluish gray. In later work Murchie and Erard (1996), using a composite spectrum from the ISM, KRFM, and VSK, condensed these four units into two main spectral units: a redder sloped "background" unit (here called Phobos red unit or PRU) and a less-red-sloped unit associated with Stickney crater (here called Phobos blue unit or PBU). The PRU consists of what was called "red" and "reddish gray" by Murchie *et al.* (1991) and the PBU consists of the former "blue" and "bluish gray" units. The PBU and PRU correspond, very roughly, to the leading (longitudes 0° – 180°) and trailing (longitudes 180° – 360°) hemispheres of Phobos, respectively. Stickney is centered near a longitude of 60° . The PBU mineralogy may represent a "fresher" (less mature) version of the PRU mineralogy, or it may represent a different mineralogy altogether, excavated by the Stickney impact. Simonelli *et al.* (1998) argued from photometric data that this difference is probably not simply a particle size effect.

Differences in visible albedo exist on Deimos as well, although these are correlated with topography rather than found in more coherent units as on Phobos (Thomas *et al.* 1996). High spatial resolution color observations of Deimos were not obtained by Phobos 2, and the Viking data which exist are in a very restricted wavelength range. The Imager for Mars Pathfinder (IMP) obtained disk-integrated, visible-range spectrophotometric data for the sub-Mars hemispheres of Phobos and Deimos (Murchie *et al.* 1999), showing the former to have colors between those of the Phobos blue and Phobos red units (presumably due to mixing between the two units) and the latter to be quite red, consistent with the results of Grundy and Fink (1992).

A $3\text{-}\mu\text{m}$ absorption feature is typically caused by a combination of the very strong OH-radical absorption feature and the very strong first overtone of the $6\text{-}\mu\text{m}$ H_2O fundamental. Adsorbed water has a symmetric stretch, giving rise to an absorption feature at $3.1\ \mu\text{m}$, and an antisymmetric stretch feature at $2.9\ \mu\text{m}$. Structural hydroxyl (OH) that has been incorporated into mineral lattices produces a stretch absorption at $2.7\ \mu\text{m}$. The depth

of the fundamental $\text{H}_2\text{O}/\text{OH}$ feature depends on many parameters besides abundance of hydrated material, including particle size, albedo, and temperature. However, water abundances as low as fractions of a weight percent are observable using $3\text{-}\mu\text{m}$ spectroscopy (Salisbury *et al.* 1991).

The Murchie and Erard spectra extend from 0.3 to $2.9\ \mu\text{m}$ for the PRU and from 0.3 to $1.0\ \mu\text{m}$ for the PBU. The PRU shows no consistently resolvable $3\text{-}\mu\text{m}$ absorption feature, which indicates little or no hydrated minerals, as detailed below. The hydration state of the PBU could not be determined given the limited spectral coverage of this unit by Phobos 2. It thus remained possible that interior hydrated minerals could have been liberated by the Stickney impact and present on the surface in that spectral unit.

Observations of Deimos in the $3\text{-}\mu\text{m}$ region were made by Bell *et al.* (1989b). They concluded that Deimos had a band depth of $5\text{--}10\%$, though they could not rule out a completely anhydrous surface. Our observations are consistent with those of Bell *et al.*, and given their relatively large uncertainties, their data support our results of an anhydrous surface for Deimos.

Observations at 4.8 , 10 , and $20\ \mu\text{m}$ were made by Veeder *et al.* (1987), who found Deimos to be brighter than expected using the physical parameters and thermal models available at the time. This work is further discussed in Section 3. More recently, the thermal emission spectrometer (TES) on Mars Global Surveyor (MGS) measured the IR spectral properties of Phobos from 5.88 to $50\ \mu\text{m}$ (Roush and Hogan 2000). Roush and Hogan found that Phobos is composed of fine-grained materials more consistent with silicates than organic refractories, which they found suggestive of formation near Mars' orbit rather than in the outer asteroid belt, although further study is under way. Finally, radar observations of Phobos were obtained by Ostro *et al.* (1989). They determined a radar albedo of Phobos of 0.093 ± 0.035 , in the range of low-albedo main-belt asteroids.

2. OBSERVATIONS

We observed Phobos and Deimos from the NASA Infrared Telescope Facility (IRTF) on Mauna Kea, Hawaii. We used NSFCAM paired with the Cold Coronagraph (CoCo) (Shure *et al.* 1994, Wang *et al.* 1994, Toomey *et al.* 1998) to facilitate IR imaging of the faint martian satellites, which are $7\text{--}8$ magnitudes fainter than Mars and in close proximity to the planet (less than ~ 20 arcsec for Phobos and ~ 50 arcsec for Deimos). Pairs of images were taken using the circular variable filter (CVF) available on NSFCAM, at wavelengths of 1.65 , 1.80 , 2.00 , 2.20 , 2.40 , 2.95 , 3.05 , 3.12 , 3.20 , 3.35 , and $3.50\ \mu\text{m}$. This coverage enabled us to cover spectral regions containing both the $2\text{-}\mu\text{m}$ pyroxene and $3\text{-}\mu\text{m}$ water of hydration absorption features, with the remaining data serving to define the continuum. Observing circumstances are provided in Table I. Observations were made on $25\text{--}26$ April 1999 (UT), although poor weather on the 25th made the data collected of limited usefulness. Only data collected on 26 April are used in this paper.

TABLE I
Observational Circumstances, 26 April 1999 UT

Body	Times (UT)	Angular distance	Δ Mag	SELat ^(c)	SELon ^(c)
Phobos (trailing)	0811–0948	22.6–14.4''	$\equiv 0$	+34.2	246.7–323.7
Phobos (leading)	1211–1316	21.7–17.5''	$+0.24 \pm 0.06$	+34.2	75.6–125.9
Deimos (leading)	1022–1133	51.9–45.9''	$+0.98 \pm 0.07$	+36.8	53.7–67.6

Note. The phase angle for the martian system was 1.6° for these observations. The angular distance is calculated from the center of Mars. During the period of observations Mars had an angular diameter of 16.1 arcsec. SELat and SELon are the sub-Earth latitude and longitude, respectively. Δ Mag is the observed magnitude difference at $1.65 \mu\text{m}$ and includes both shape and albedo effects.

Operationally, CoCo is inserted into the IRTF beam before NSFCAM. Light from the IRTF secondary first passes through user-selectable slits external to CoCo. Upon entering CoCo, the light is collimated and passed through focal plane masks and a 77 K pupil mask specially designed to reject light from the periphery of the IRTF primary and secondary, as well as scattered light from the secondary mirror support structures (Wang *et al.*

1994, Toomey *et al.* 1998). Light that passes through the pupil mask is sent through a reimaging lens and becomes the input beam to NSFCAM. For our observations we used two special focal plane masks with either a 4'' or 10'' back-beveled and knife-edged central hole designed for previous CoCo observations of the faint inner jovian satellites (Bustani *et al.* 1997). These “puka” (Hawaiian for “hole”) masks provide additional

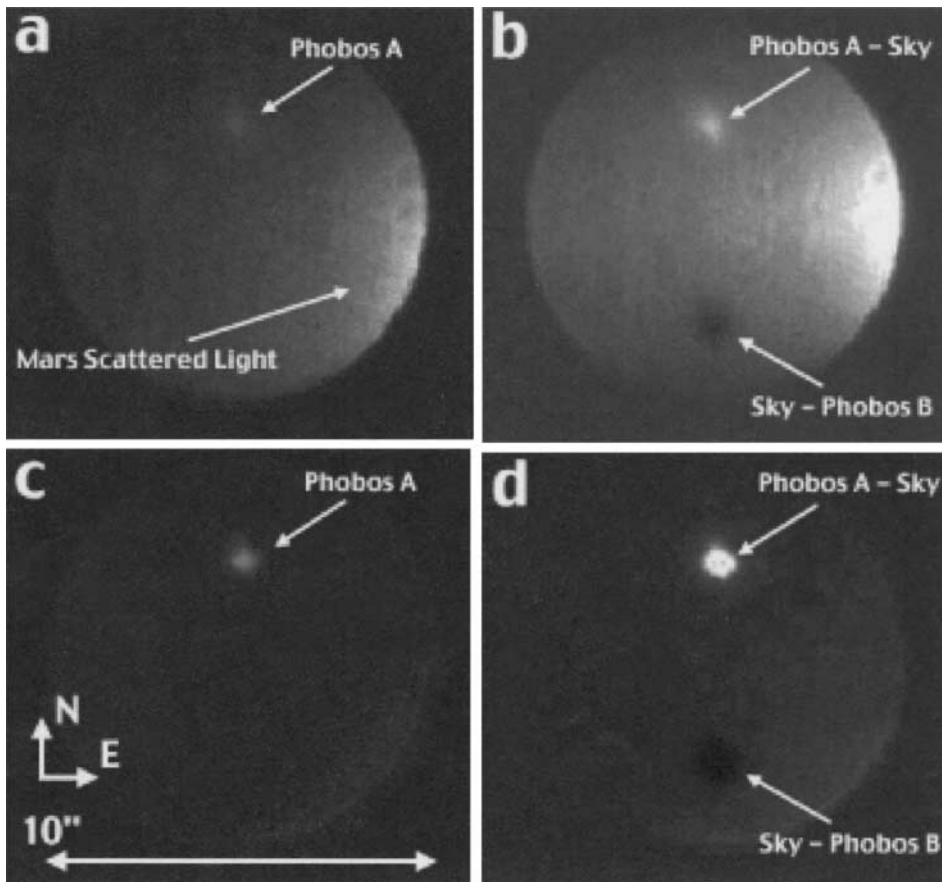


FIG. 1. Original and processed IRTF NSFCAM/CoCo images of Phobos. (a) “A beam” image at $1.65 \mu\text{m}$, taken when Phobos was 8.1 arcsec from the limb of Mars. (b) Difference image between the A beam and the B beam, which was taken after offsetting the telescope by 5 arcsec north. The A – B subtraction removes contributions from the sky and dark counts and also yields a second (negative) image of Phobos for data analysis. These frames show evidence for residual scattered Mars light fairly close to Phobos. (c) Similar to (a) except obtained when Phobos was 12.2 arcsec from the limb of Mars. (d) Corresponding A – B difference image for (c). There is little or no scattered light contribution from Mars evident in these images. The NSFCAM focal plane mask hole (“puka”) is 10 arcsec across, and the plate scale of the images of 0.055 arcsec per pixel. North is up and east is to the right.

suppression of off-axis or scattered light from the bright primary before it enters CoCo (Fig. 1). The observations reported here all used the 10'' puka.

Pairs of images were taken at each wavelength to perform a sky and dark correction. The pairs of images were taken within 2 min (commonly less) of each other, so the corrections are near-simultaneous. The filter sequence was repeated several times using relatively short exposures (between 20 and 120 s total integration per image for Phobos and between 30 and 200 s for Deimos) to characterize and correct for lightcurve effects. We used a small throw (5 arcsec between the two beams in each pair) to remain within the puka and double the amount of data obtained. Because the data are images, scattered light from Mars was easily characterized, and images containing excessive amounts of scattered light were rejected. Typically, martian scattered light was a greater problem at the shortest wavelengths ($\lambda < 2.7 \mu\text{m}$) where we obtained data, because Mars itself has a strong 3- μm hydrated mineral band. The Phobos spectra reported in this paper were all taken near elongations (11–14 arcsec from Mars' limb), where scattered light contributed very little (see Fig. 1). Given the strong 2- μm absorption feature found in martian spectra (due to CO_2 in its atmosphere) and the lack of such a feature in our Phobos spectra, significant scattered light from Mars is unlikely to be present in these data. The same conclusion can be derived from the difference between Mars' flat spectral slope in the 1.5–2.5 μm region compared to the steeply sloped satellite spectra. Deimos was between 35 and 40 arcsec from the limb of Mars during observations. Synthetic aperture photometry was performed using the IRAF apphot packages (Tody 1986).

We also observed SAO 158412, a star within a degree of the satellites' position, with airmasses bracketing the satellite observations. This star's spectral type is G1V (Houk and Swift 1999) and was used to correct the martian satellite data for solar colors.

3. THERMAL CORRECTIONS

Phobos and Deimos, at a distance of 1.59 AU from the Sun at the time of these observations and with relatively low albedos, have significant thermal fluxes longward of 3 μm which must be modeled and removed to get the true reflectance spectra. Previous studies of the martian satellites have resulted in well-constrained quantities for albedo, size, and thermal inertia. We used a thermophysical model described in Lebofsky and Spencer (1989) to calculate and remove the thermal flux from Phobos and Deimos. We note that while most quantities input to the thermal models are well constrained, there remains one, the "beaming parameter" (β), which is not. The beaming parameter represents the suite of effects not explicitly included in the standard thermal model (STM), such as nonspherical shapes and thermal inertia. While β cannot be derived for a given asteroid from first principles, it can be fit from data, with a value usually between 0.7 and 1.2. Using radiometry of Deimos performed by Veeder *et al.* (1987), β can be estimated. Although Veeder *et al.*

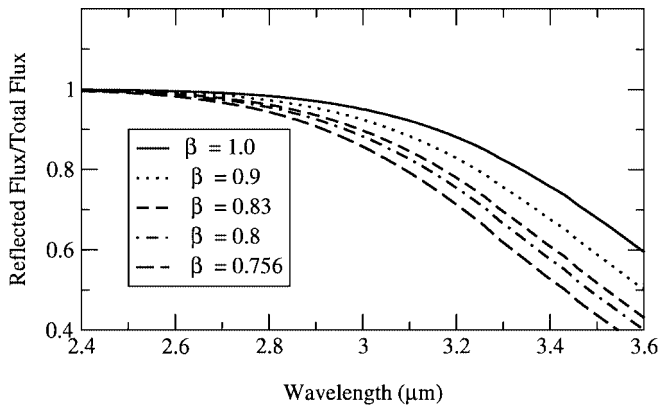


FIG. 2. The effect of the beaming parameter on Phobos thermal models. The beaming parameter (β) is included in asteroid thermal models to account for surface roughness and other factors not easily modeled. A value of 0.756 for β was recommended by Lebofsky and Spencer (1989) for use with asteroid thermal models. Radiometric observations of Deimos by Veeder *et al.* (1987) are better fit by values of β between 0.8 and 0.85. The models shown all are for a Phobos-sized body 1.59 AU from the Sun with an albedo of 0.071. Values of β between 0.9 and 0.756 result in a spread of thermal corrections that differ by less than 10% near 3 μm , and the Deimos-derived constraint on β makes the uncertainties in the thermal correction smaller than the observational uncertainties.

were unable to find a satisfactory thermal model for Deimos, revised values for Deimos' geometric albedo, phase integral, and absolute magnitude are all now available (Thomas *et al.* 1996) and were used in this work. We find that a value for β between 0.8 and 0.85 provides the best fit for the data of Veeder *et al.*, although their value for Deimos' N magnitude in 1986 cannot be fit within the quoted uncertainties.

We thus used a value of 0.83 for β . This value is close to 0.756, the value found for the asteroids Ceres and Pallas and suggested by Lebofsky and Spencer (1989) for use with most asteroids. The effect of increasing β is to decrease the thermal correction. However, given the constraints from Veeder *et al.* (1987), we did not explore large areas of parameter space for β . As a guide to the effect of different values of β upon the thermal correction, Fig. 2 shows thermophysical models (described in more detail in the following) calculated for Phobos at a distance of 1.59 AU from the Sun, with the nominal thermal inertia from Ksanfomality *et al.* (1991), an albedo of 0.071 (Simonelli *et al.* 1998), and values of β ranging from 0.756 to 1.0. The reflectance at 2.5 μm is also used in the model to account for large continuum slopes. As can be seen, the effect can be large at the longest wavelengths available in our data but is only about 10% of the correction near 3 μm , the area of greatest interest. It can also be seen that a false detection of a 3- μm hydration feature due to incorrect thermal subtraction would be accompanied by a steep downward slope longward of 3 μm , which is not present in our data. Furthermore, it is obviously impossible to remove a feature which is present by performing an incorrect thermal subtraction.

The thermal parameter (Θ), described in Lebofsky and Spencer (1989) and Spencer (1990), provides a means for determining whether a body can be fit with the STM or whether

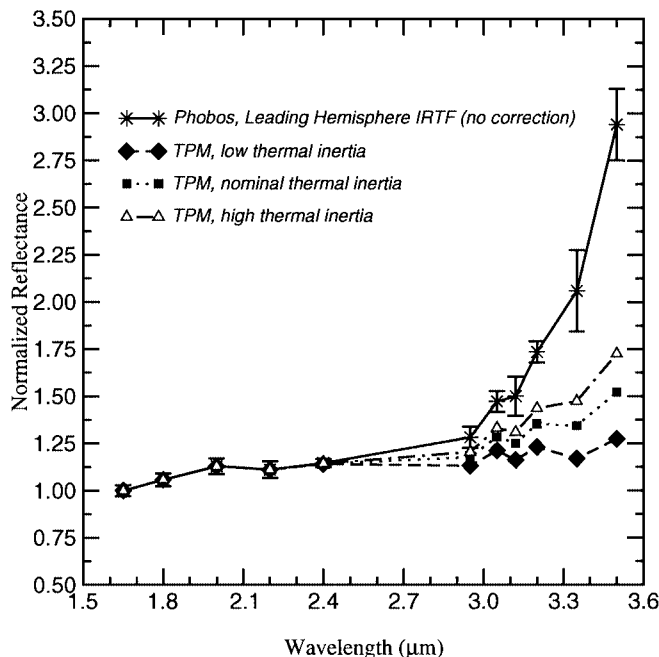


FIG. 3. Comparison of thermal corrections for the leading hemisphere of Phobos. Illustrated here are the effects of various thermal corrections on the data. The quoted value for Phobos' thermal inertia is 0.002 ± 0.001 cal/(cm² deg s^{1/2}). These models are for the nominal value and 1- σ values of thermal inertia. The two 1- σ models differ from the nominal model by less than 4% at 2.95 μ m, the region of greatest interest. The nominal value of thermal inertia is used for models in this paper. Error bars for the thermally corrected points are the same as for the uncorrected data and are omitted for clarity.

a more sophisticated thermophysical model is necessary, based on thermal inertia (known or estimated), distance from the Sun, size, and rotation period. If $\Theta < 0.1$, the STM can be used, while $0.1 < \Theta < 10$ indicates that thermophysical models are more appropriate. While the STM is sufficient for correcting the Deimos data ($\Theta \sim 0.06$), it will not work for Phobos ($\Theta \sim 0.44$). This difference in thermal parameters between Phobos and Deimos is due almost entirely to the difference in orbital periods and to Phobos' somewhat higher thermal inertia (Lunine *et al.* 1982).

We have therefore run separate thermophysical models for the blue and red unit of Phobos using the nominal value of Phobos' thermal inertia given in Ksanfomality *et al.* (1991) of 0.002 ± 0.001 cal/(cm² deg s^{1/2}) and albedo values estimated using Fig. 5 in Simonelli *et al.* (1998) of 0.062 and 0.075 for the PBU and PRU, respectively. Uncertainties in thermal inertia can result in up to a 35% spread in flux correction at longest wavelengths but only a 10% spread at 2.95 μ m (see Fig. 3). In subsequent figures, the spectra shown have been thermally corrected using this thermophysical model with the nominal thermal inertia for Phobos and the STM for Deimos.

4. SHAPE AND PHOTOMETRY CORRECTIONS

Because the IRTF data are spectrophotometric, we can determine the relative fluxes of the two sides of Phobos for each

wavelength and therefore correctly scale the leading side spectrum to the trailing side spectrum, as further detailed below. To do this, of course, we must account for differences in shape between the two sides. Using the Simonelli *et al.* (1993) shape model, we calculated the expected relative fluxes based on shape alone, knowing that the residual differences must be due to albedo. The cross-sectional area varies only by 2–3% during the time of our observations, and, as this correction is smaller than our typical uncertainty, it is neglected. Similarly, given the known shapes and sizes of Phobos and Deimos we can determine the relative reflectances of Phobos and Deimos at any wavelength in our data. We do not include the effect of shadows, but because the phase angle of the observations was only 1.6°, the effect will be negligible. Similarly, phase reddening is not important this close to opposition. The Phobos 2 ISM observations of the PRU were at higher phase angles (28°–31.5°). However, the photometric work of Cantor *et al.* (1999) suggests that the phase coefficients are not strongly wavelength-dependent (within 10%) in the visible and near IR. Furthermore, because reflectance is changing slowly with wavelength beyond 1.6 μ m for Phobos and Deimos, their phase coefficients will be nearly constant at those wavelengths (Gradie and Veverka 1986).

5. RESULTS

5.1. Phobos

Figure 4 shows the relative reflectances from 1.65 to 3.5 μ m for the leading and trailing sides of Phobos and for 1.65 to 3.12 μ m for Deimos. These reflectances are normalized to the 1.65- μ m flux of the trailing hemisphere of Phobos. The leading hemisphere of Phobos is fainter than the trailing side, due to the different spectral units dominating each hemisphere. Deimos is fainter due to its smaller size, although as shown below its spectral slope is comparable to that of the Phobos trailing unit. The relative magnitudes at 1.65 μ m of the leading and trailing sides of Phobos and Deimos are shown in Table 1.

Figure 4 also shows that the spectra of the trailing and leading sides of Phobos look similar when they are normalized to 1.65 μ m. The spectral slopes are the same within observational uncertainties, and neither side shows evidence of a 3- μ m hydration feature within 5–8%. For comparison, CI chondrites have 10–20% water, and CM chondrites have 5–10% water (Lewis *et al.* 1993), which results in 3- μ m band depths upward of 50%. It is clear that the surface of Phobos has much fewer hydrated minerals than the aqueously altered carbonaceous chondrites, and it may have none at all.

There also is no evidence for a 2- μ m pyroxene feature on Deimos or on either side of Phobos within 4–5%, as also noted by Murchie and Erard (1996). Again, this cannot be directly used to determine a limit on the surface fraction of pyroxene due to the aforementioned factors, including the fact that the iron-free endmember of pyroxene shows no 2- μ m absorption

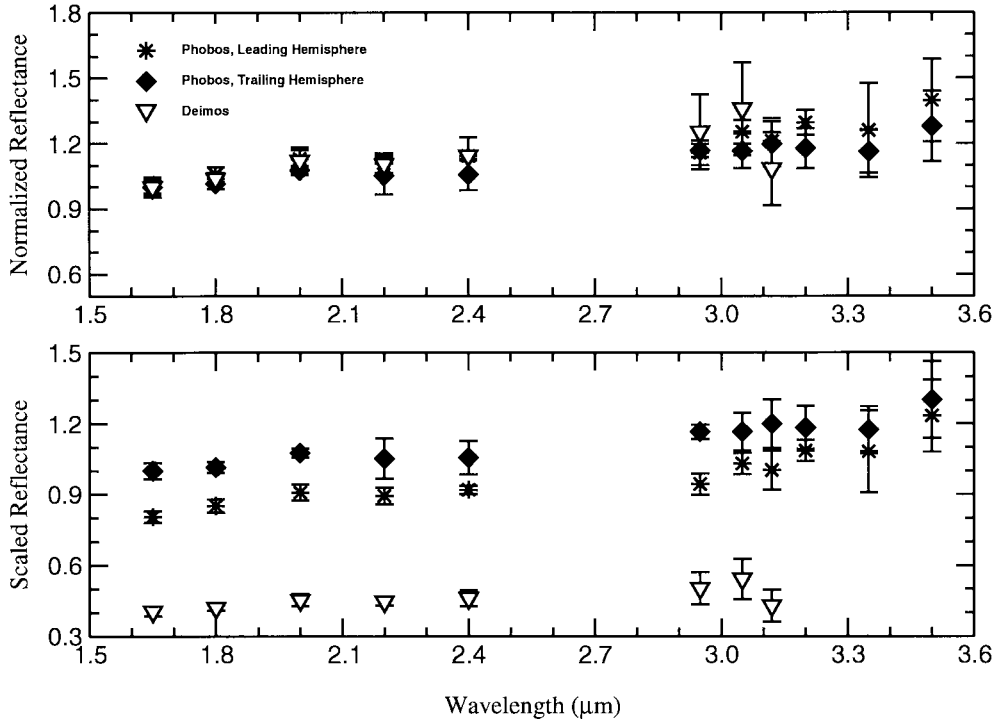


FIG. 4. (Top) The trailing and leading hemispheres of Phobos, along with Deimos, normalized to equal 1 at $1.65 \mu\text{m}$. These have the same colors in the $1.65\text{--}3.5 \mu\text{m}$ region within observational uncertainties. (Bottom) The relative reflectances of the trailing and leading hemispheres of Phobos, scaled so that the trailing hemisphere reflectance equals 1 at $1.65 \mu\text{m}$. The leading side of Phobos is nearly 20% fainter at $1.65 \mu\text{m}$ than the trailing side, although their cross-sectional areas are nearly the same. This is because the albedo of the PBU, which dominates the leading side, is lower than that of the PRU at this wavelength. Deimos, on the other hand, is fainter than Phobos because of the difference in size, rather than albedo. This and all following figures have been thermally corrected.

feature. However, the ordinary chondrite meteorites have a $2\text{-}\mu\text{m}$ band depth around 10% (Gaffey 1976), and S asteroids a band depth of 5–10% (Bell *et al.* 1988) as a means of comparison.

To compare our data to previously obtained data, we used the value of $R_{1.65 \mu\text{m}}/R_{0.55 \mu\text{m}}$ found by scaling our Phobos trailing hemisphere data to the Phobos red unit spectrum of Murchie and Erard (1996) from 1.65 to $2.40 \mu\text{m}$ and then determined $R_{1.65 \mu\text{m}}/R_{0.55 \mu\text{m}}$ for the Phobos leading hemisphere and Deimos using the relative fluxes shown in Fig. 4. We also determined the value of $R_{1.65 \mu\text{m}}/R_{0.55 \mu\text{m}}$ for our measurements of the PRU (with longitude bounds as described below) by scaling to the PRU spectrum of Murchie and Erard (1996). Although technically the trailing side spectrum and PRU spectrum are not identical because the trailing side spectrum contains a small contribution from the PBU, the errors introduced are only on the order of 2–3%.

5.1.1. Determining the PRU. The subset of trailing side data near central longitudes 218° to 279° is almost entirely covered by the red unit (S. Murchie, personal communication), so these data were defined as the Phobos red unit for these calculations. This subset of the CoCo data and the Phobos 2 ISM data are in excellent agreement (see Fig. 5) after normalization. For comparison, data in the $0.4\text{--}1.1 \mu\text{m}$ region were

obtained by Phobos 2 for the longitude range $30^\circ\text{--}250^\circ$, while data longward of this were only available for a region of the trailing hemisphere solely containing the PRU and centered farther south than our observations. Although the phase angle of the Phobos 2 observations was also much higher than that of our observations, the excellent agreement between the Phobos 2 and IRTF data after normalization shows that the phase coefficient of Phobos does not change much with wavelength in the area of overlap between the data sets (between 1.65 and $2.95 \mu\text{m}$). This is consistent with asteroidal data (Veeder *et al.* 1978).

5.1.2. Calculating the PBU spectrum. Although the Phobos 2 data did not cover this set of latitudes, the fractional coverage of the red unit can be estimated for the leading side at sub-Earth latitude of $\sim 30^\circ\text{N}$ ($\sim 33\text{--}50\%$: S. Murchie, personal communication).

The reflectance of the leading hemisphere of Phobos is a weighted average of the contributions of the Phobos red and Phobos blue units,

$$R_{\text{leading},\lambda} = f \times R_{\text{red},\lambda} + (1 - f) \times R_{\text{blue},\lambda}, \quad (1)$$

where f is the fraction of Phobos' leading hemisphere covered

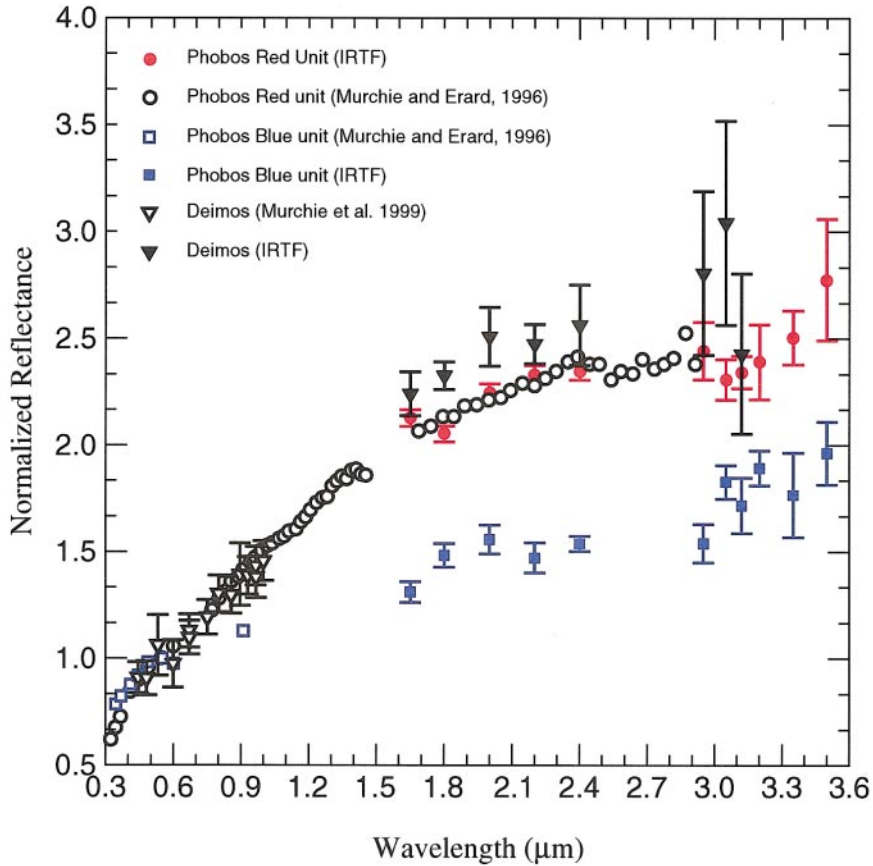


FIG. 5. The 0.3–3.6 μm spectra of Phobos and Deimos, integrating data from Murchie and Erard (1996), Murchie *et al.* (1999), and this work. In this and following figures, the data obtained in this work have been normalized so that the PRU spectrum matches the Phobos 2 ISM data from Murchie and Erard (1996) in the 1.65–2.40 μm region.

with the PRU. Because $R_{\text{leading},\lambda}$ and $R_{\text{red},\lambda}$ have been measured (in this work and Murchie and Erard (1996), respectively), $R_{\text{blue},\lambda}$ is calculable using the estimates for f .

Figure 6 shows the results of this unmixing. A model assuming a 1 : 2 mixture of the red and blue units on the leading side of Phobos is used in following figures, except where noted. The 1 : 2 model is chosen because its slope extrapolated to shorter wavelengths comes quite close to the PBU data from Murchie and Erard (1996), especially compared with the other mixing models. A 1 : 2 model is also consistent with previous estimates of the relative PBU/PRU coverage of this area (S. Murchie, personal communication). This is obviously not a unique solution, and further observations at other aspects will help refine the PBU spectrum. Our conclusions do not depend upon the exact choice of model.

Because the PBU has never been observed in the infrared prior to this work, the possible phase reddening behavior of this unit is unknown. However, given the lack of appreciable phase reddening of the PRU and the lack of phase reddening in this wavelength region found on asteroids by Veeder *et al.* (1978), combined with the relatively small difference in phase angle between our observations of the PBU and those of Phobos 2, we can safely neglect this effect.

5.2. Deimos

Because of our intention to concentrate on obtaining data for Phobos, Deimos was only observed during times when Phobos was too close to Mars for usable data to be obtained. As a result, Deimos was observed in a restricted wavelength range compared to Phobos. Although our coverage of Deimos only extends to 3.12 μm , it also looks similar to the two hemispheres of Phobos when normalized to 1.65 μm , in agreement with previous observations (Bell *et al.* 1989b). Grundy and Fink (1992) observed Deimos in 1988, when Deimos was at nearly the same sub-Earth longitude as in our observations. The Grundy and Fink spectrum is nearly identical to the PRU spectrum of Murchie and Erard in the area of overlap (0.3–1 μm), as are the Deimos data obtained by Murchie *et al.* (1999).

Because there is no data set available for Deimos with which our data set overlaps, and because we lacked an independent measure of the visible flux of Deimos at the time of our observations, it was necessary to bootstrap from the Phobos data to obtain a full visible and near-IR spectrum of Deimos. We determined $R_{1.65\mu\text{m}}/R_{0.55\mu\text{m}}$ for Deimos in the following manner: Given the known sizes and shapes of Phobos and Deimos (Simonelli *et al.* 1993), we were able to determine the magnitude

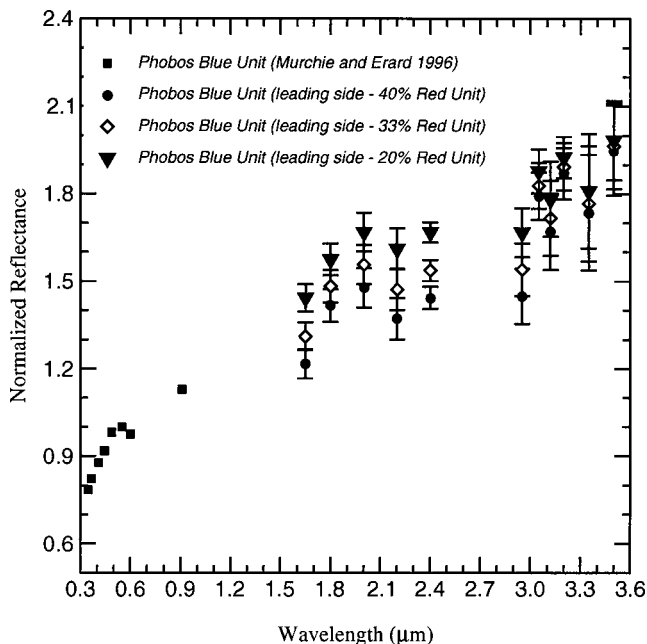


FIG. 6. Derived spectra for the PBU. Because the PRU and PBU exhibit areal mixing on the scale visible from Earth, the PBU can be derived from subtracting the appropriate fraction of Phobos red from the trailing or leading hemisphere data. Here, a subset of the trailing hemisphere data was known to be covered entirely with the PRU. This was defined as the PRU and was subtracted from the rest of the leading hemisphere data. The model assuming a 1 : 2 PRU : PBU mixture for the leading side results in a spectral slope which when extrapolated to shorter wavelengths matches the PBU spectral slope from Murchie and Erard (1996). This ratio is therefore preferred, although it is nonunique. A 1 : 2 ratio of PRU : PBU for the leading hemisphere is in agreement with prior estimates.

difference that was due to cross-sectional area alone at the time of our observations. This was subtracted from the measured magnitude difference at $1.65 \mu\text{m}$, leaving the difference due to albedo differences at that wavelength. This is easily converted to $R_{1.65 \mu\text{m, Deimos}}/R_{1.65 \mu\text{m, Phobos}}$. Given the known spherical albedos of Phobos and Deimos (Thomas *et al.* 1996, Simonelli *et al.* 1998), we were able to obtain $R_{1.65 \mu\text{m}}/R_{0.55 \mu\text{m}}$ for Deimos relative to Phobos. The calculated value for $R_{1.65 \mu\text{m}}/R_{0.55 \mu\text{m}}$ for Deimos is 2.21, similar to that of the red unit of Phobos, or perhaps even redder still. The resulting spectrum for Deimos, along with those for the red and blue units of Phobos, is shown in Fig. 5. We note that the uncertainties in $R_{1.65 \mu\text{m}}/R_{0.55 \mu\text{m}}$ have not been included in the error bars for Deimos on this figure, but these are dominated by the errors already present in the Deimos spectrum.

6. DISCUSSION

6.1. Comparisons with Meteorites

Searching for analogs for the composition of the martian satellites, we look to meteorites present on the Earth. No meteorites have published spectra similar to the red unit of Phobos or

Deimos, both of which are much redder than the meteorites. Therefore, in searching for a good analog for the martian satellites, we must look for good matches to the Phobos blue unit, although because its spectrum was derived rather than directly measured, the uncertainties may be greater. A discussion of possible meteorite analogs to the Phobos red unit was included in Murchie and Erard (1996).

Carbonaceous chondrites were considered good analogs for the martian satellites by earlier workers (Pang *et al.* 1978, Pollack *et al.* 1978). However, the work done by Grundy and Fink (1992) and Murchie and Erard (1996), among others, showed that the continuum slopes of the satellites were in general much too high to match these meteorites, as mentioned above. The lack of a $3\text{-}\mu\text{m}$ feature on the PBU seems to preclude identification with the CM and CI meteorites, which are rich in phyllosilicates and other products of aqueous alteration. Thermally metamorphosed CI/CM meteorites, studied by Hiroi *et al.* (1996), can be close in spectral shape, but they also have $3\text{-}\mu\text{m}$ features, although these are weaker than those of CI/CM meteorites (Fig. 7). The best match to the PBU seems to come from strongly heated carbonaceous chondrites, also studied by Hiroi *et al.* (1996). Figure 7 shows the PBU compared to a sample of the CM chondrite Murchison heated to 700°C . At this temperature, the hydrated minerals abundant in Murchison have been almost completely destroyed, and the spectrum reflects an anhydrous appearance. When the meteorite is heated to higher

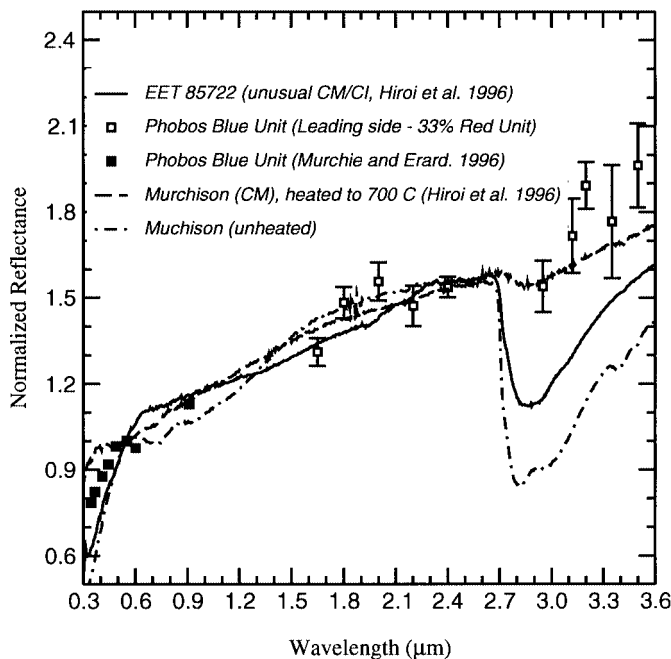


FIG. 7. Comparison of PBU to possible meteorite analogs. The best meteoritic spectral analogs to the PBU appear to be thermally metamorphosed CI/CM meteorites, although these still have a much stronger $3\text{-}\mu\text{m}$ feature than is indicated on Phobos. Murchison, a CM chondrite, provides a good spectral match after it has been heated to 700°C . The spectrum of an unheated specimen of Murchison is also shown. The meteorite spectra are from Hiroi *et al.* (1996).

temperatures, the spectral slope decreases, and its similarity to Phobos becomes less obvious.

6.2. Comparison with Other Bodies

6.2.1. Asteroids. It has been noted that the D-class asteroids, which also have very red continua and in general lack a $3\text{-}\mu\text{m}$ feature (Jones *et al.* 1990), are close spectral matches to Deimos and Phobos (Grundy and Fink 1992). This leads to the supposition that Deimos and Phobos are captured bodies originally from the outer asteroid belt, which is dominated by D-class asteroids (Gradie *et al.* 1989). However, the stability of the orbits of Phobos and Deimos is inconsistent with a capture origin (Burns 1992). Outer-belt asteroids are thought to be mixtures of anhydrous silicates and interior ice which never got warm enough to melt and react to form hydrated minerals (Jones *et al.* 1990; Bell *et al.* 1989a). If Phobos and Deimos were of that composition, they could have been warm enough at a semi-major axis of 1.5 AU to melt internal ice, experience aqueous alteration, and show spectral features of hydrous minerals. Maturation effects could plausibly devolatilize the surfaces of Phobos and Deimos. Although data on impact dehydration of phyllosilicates are limited (Boslough *et al.* 1980, Thibault *et al.* 1997), they suggest that much (though not all) of the water in phyllosilicates will remain after impact. While it is naive to assume that the spectrum of the optical surface of a body is inevitably representative of a body as a whole, neither should we assume that the lack of a $3\text{-}\mu\text{m}$ feature on both the more- and less-weathered spectral units of Phobos is irrelevant to the water budget of the martian satellites. The lack of a $3\text{-}\mu\text{m}$ absorption feature on Phobos and Deimos is unlikely to have the same explanation as the lack of these absorption features on the typical outer-belt D-class asteroids.

D-class asteroids typically have albedos lower than that of Phobos (3–5% versus 7% for the PBU; Tedesco *et al.* 1992). Diagnostic absorption features are not present for D-class asteroids. A comparison of the D-class asteroids 336 Lacadiera and 1867 Deiphobus to Phobos and Deimos is made in Fig. 8. The asteroid 336 Lacadiera compares reasonably well with the PBU and is one of the least red of the D asteroids. Interestingly, it has a semi-major axis of 2.25 AU (considered to be the inner belt), while 26 of the 32 D asteroids are in the outer belt Cybele (~ 3.4 AU) and Hilda (~ 4 AU) regions or the Trojan clouds of Jupiter (~ 5.2 AU). Also, 336 Lacadiera seems to show some evidence of variation in the $3\text{-}\mu\text{m}$ region, with one set of observations showing a hydration feature (Howell 1995). Because it has a $3\text{-}\mu\text{m}$ feature, Lacadiera is unrepresentative of D-class asteroids in general. It is uncertain whether the presence of hydrated minerals on this body is evidence of a composition different from outer-belt D-class asteroids or whether Lacadiera merely has a different thermal history resulting from its placement in the inner belt. Figure 8 shows observations of 336 Lacadiera without the $3\text{-}\mu\text{m}$ absorption feature. The asteroid spectra in this and the following figure are compilations of data from the Eight

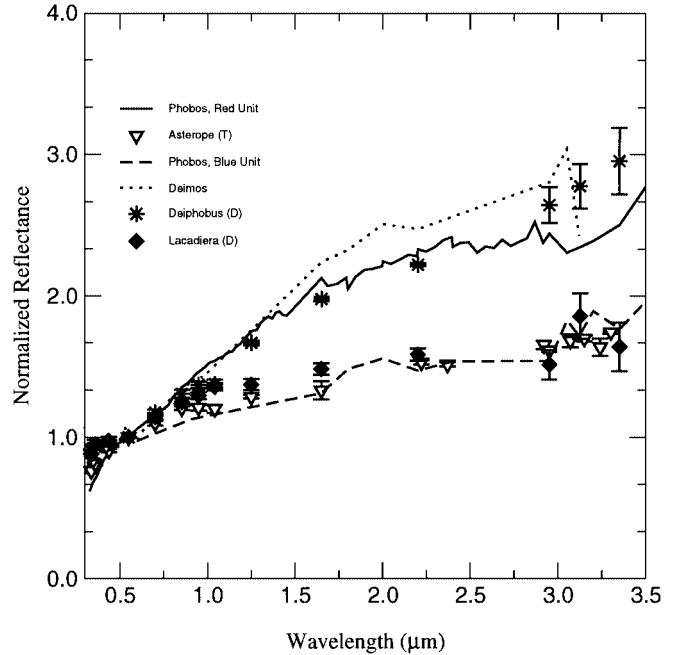


FIG. 8. Comparison of Phobos and Deimos to possible Asteroid analogs. The D-class asteroids dominate the Trojan clouds of Jupiter and the outer asteroid belt. They are thought to be organic-rich bodies with unreacted interior water ice. Most D asteroids, including the Trojan asteroid 1867 Deiphobus, have anhydrous surfaces, but 336 Lacadiera, the D asteroid with the smallest semi-major axis, shows evidence of hydrated minerals on some faces. The observation shown is anhydrous. Although the D asteroids are qualitatively consistent with the PRU, PBU, and Deimos longward of $0.55\ \mu\text{m}$, the match shortward of that wavelength is poor at best. The T class is a spectral type with no agreed-upon composition, but possibilities include heavily thermally metamorphosed carbonaceous chondrites or troilite. The PBU is matched well by T-class asteroids, here represented by 233 Asterope. The martian satellite spectra are the combined data of Murchie and Erard (1996) and this work for Phobos and Murchie *et al.* (1991) and this work for Deimos. The asteroid spectra in this figure are compilations of data from the Eight Color Asteroid Survey (Zellner *et al.* 1985), the 52-Color Survey (Bell *et al.* 1988), and $3\text{-}\mu\text{m}$ data from Jones *et al.* (1990), Lebofsky *et al.* (1990), and Howell (1995) as resampled by Merényi *et al.* (1997).

Color Asteroid Survey (Zellner *et al.* 1985), the 52-Color Survey (Bell *et al.* 1988), and $3\text{-}\mu\text{m}$ data from Jones *et al.* (1990), Lebofsky *et al.* (1990), and Howell (1995) as resampled into 14 channels by Merényi *et al.* (1997). The fact that D-class asteroids span the range of spectra from the PBU to the PRU is interesting and worth exploring, but the only true connection between the red unit of Phobos and the Trojan asteroids may be that they both have spectra that are featureless in similar ways. Alternately, the common interpretation of outer-belt asteroids containing ice-rich interiors may be incorrect.

The lack of asteroids in the outer belt and Trojan clouds with spectra like the blue unit of Phobos (Gradie *et al.* 1989) is circumstantial evidence against Phobos and Deimos originating in the outer asteroid belt. Given the presence of both the PBU and PRU on a single body, spectra similar to both spectral units would be expected among the source population of Phobos and

Deimos. The apparent lack of such a population in the outer belt could also plausibly be due to incomplete sampling of the outer belt.

The PBU is well matched by T-class asteroids, which constitute a rare mid-belt spectral class. The T-class asteroids have been proposed to be troilite (Britt *et al.* 1992), or highly metamorphosed carbonaceous chondrite material (Bell *et al.* 1989a), but no consensus has been reached, and indeed the T class may contain a number of unrelated mineralogies. Figure 8 shows the Deimos, PRU, and PBU data compared to the T asteroid 233 Asterope.

There have been at least two Mars Trojan asteroids discovered, with two others pending confirmation (Tabachnik and Evans 1999). The spectrum for one of them, 5261 Eureka, places it in the S class of asteroids, which is quite dissimilar to Phobos and Deimos (Howell *et al.* 1995). We must conclude that at least 5261 Eureka and the martian satellites have different origins.

6.2.2. The moon. Lunar spectra can be found which match both the PRU/Deimos and PBU spectra reasonably well, as shown in Fig. 9 (although the match becomes poorer longward of about $2.4 \mu\text{m}$). This was first shown by Murchie and Erard (1996). The PBU can be matched about as well. Both lunar spectra in Fig. 9 are derived from highland soils collected by Apollo 16. This suggests that the spectral alteration process on

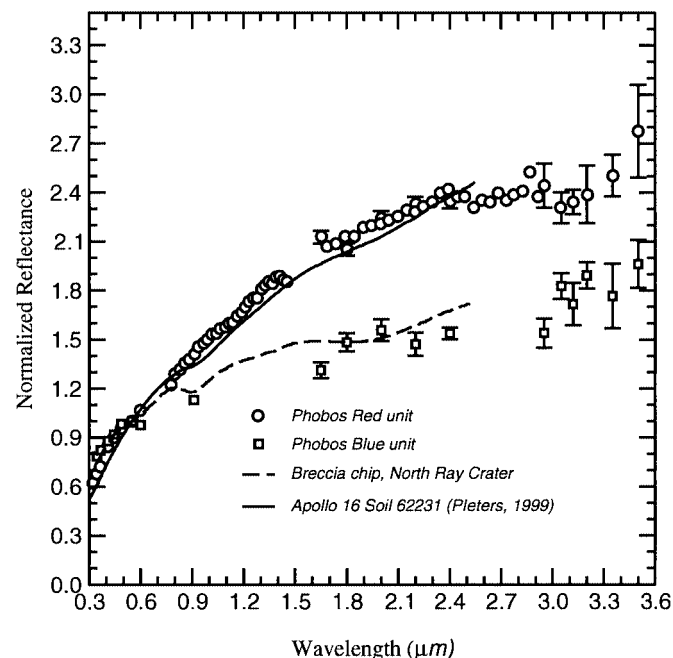


FIG. 9. Comparison of Phobos spectral units to lunar spectra. The lunar soil 62231, from Pieters (1999), was collected during the Apollo 16 mission. The spectrum of the North Ray breccia chip, also collected during the Apollo 16 mission, is from the PDS spectroscopy subnode. The martian satellite spectra are the combined data of Murchie and Erard (1996) and this work for Phobos and Murchie *et al.* (1991) and this work for Deimos.

the two bodies (and presumably Deimos as well) may be similar. However, lunar soil spectra taken by Pieters (1999) and telescopic data from McCord *et al.* (1981) both show deviation from the Phobos data, with the PRU spectrum leveling off near $2.4 \mu\text{m}$ compared to the trend of the lunar spectra. Although uncorrected thermal flux in the lunar spectra could cause these differences, this was accounted for in McCord *et al.* (1981) and is not a problem in the laboratory spectra of Pieters (1999). It should also be noted that the albedos of the lunar samples can be significantly higher than that of Phobos. While the match is as good as or better than the D/T asteroid match, it cannot be concluded at this point that the martian satellites have a lunar-soil-like composition. We also note that the minerals found in the lunar highlands are thought to be the result of a magma ocean stage, which would not be expected on bodies as small as Phobos and Deimos. Mare soils which match the PRU can be found but mare rocks with spectral slopes close to the PBU all have olivine and pyroxene absorption features many times deeper than the upper limits found on Phobos and Deimos.

7. CONCLUSIONS

We make the following conclusions from our data and analysis:

- We confirm the existence of large-scale (hemispheric) spectral heterogeneity on Phobos and have obtained the first infrared ($1.65\text{--}3.5 \mu\text{m}$) spectrophotometry of the bluer spectral unit first reported by Murchie and Erard (1996).
- We confirm the anhydrous nature of at least the surfaces of Phobos and Deimos, placing limits on $3\text{-}\mu\text{m}$ band depth of roughly 5% for both the trailing and leading hemispheres of Phobos, 5–10% for the PRU and PBU, and 10–20% for Deimos.
- We find no evidence of a $2\text{-}\mu\text{m}$ pyroxene absorption feature on Phobos to within 4–5%, in agreement with the findings of Murchie and Erard (1996). The upper limit for the amount of pyroxene present depends upon the pyroxene composition assumed but is certainly less than is found in the ordinary chondrite meteorites.
- Spectral analogs for the martian satellites are difficult to find in the asteroid belt. The outer-belt D asteroids have spectra which bracket both spectral units on Phobos and Deimos, while for the PBU the T-class asteroids also provide a good match. The unusual, thermally metamorphosed CI/CM chondrites and lab-heated carbonaceous chondrites measured by Hiroi *et al.* (1996) are the best meteorite analogs for the PBU, but there are no good meteorite analogs for either the PRU or Deimos. Lunar highland spectra can match both the PBU and the PRU shortward of $2.4 \mu\text{m}$, but the lunar behavior longward of that wavelength is not well known, and the albedo match is poor. Lunar mare rocks have 1- and $2\text{-}\mu\text{m}$ features much deeper than those seen on the martian satellites, while mare soils are too red to match the PBU.

- Spectral analogs for the martian satellites can be identified, but arguments can be made *against* most of the best ones. Hydrated minerals can be expected to form if an ice-rich outer-belt asteroid (like a D-class asteroid) were captured into orbit around Mars, although models of the internal structure of outer-belt asteroids are necessarily uncertain. Lunar highland materials are derived from igneous processes not expected on a body as small as Phobos or Deimos. No such objections exist for heated/metamorphosed carbonaceous chondrites.

- The lack of detectable amounts of hydrated minerals argues against large amounts of internal ice, which would be expected with the model of Fanale and Salvail (1989) and thus favors macroporosity effects being responsible for the low density of the martian satellites.

- The lack of detectable amounts of hydrated minerals is inconsistent with an origin for the martian satellites in the outer asteroid belt, given current understanding of the interior of outer-belt asteroids. Alternatively, outer-belt asteroids may have much less internal ice than is currently believed. If Phobos and Deimos originated in the outer asteroid belt, bodies with spectra similar to the Phobos blue unit should be found there as well, presumably at smaller sizes.

ACKNOWLEDGMENTS

ASR acknowledges support from Grant NAG5-10328. DET acknowledges support from a NASA GSRP grant and from Doug Lin and Peter Bodenheimer. The telescope operators at the IRTF were indispensable. The ephemerides for Phobos and Deimos were taken from the JPL Horizons ephemeris generator, and the ADS Abstract Service was used to help prepare the reference list. Thanks are owed to Scott Murchie for providing the ISM and IMP spectra, Peter Thomas for providing the shape models for the martian satellites, and Will Grundy for providing his Deimos spectrum. Reviews by Stephane Erard, Scott Murchie, and Carle Pieters greatly improved the manuscript.

REFERENCES

Avanesov, G., B. Zhukov, Y. Ziman, V. Kostenko, A. Kuzmin, V. Muravev, V. Fedotov, B. Bonev, D. Mishev, D. Petkov, A. Krumov, S. Simeonov, V. Boycheva, Y. Uzunov, G. G. Weide, D. Halmann, W. Possel, J. Head, S. Murchie, Y. G. Schkuratov, R. Berghanel, M. Danz, T. Mangoldt, U. Pihan, U. Weidlich, K. Lumme, K. Muinonen, J. Peltoniemi, T. Duxbury, B. Murray, K. Herkenhoff, F. Fanale, W. Irvine, and B. Smith 1991. Results of TV imaging of Phobos—experiment VSK-Fregat. *Planet. Space Sci.* **39**, 281–295.

Bell, J. F., P. D. Owensby, B. R. Hawke, and M. J. Gaffey 1988. The 52-color asteroid survey: Final results and interpretation. *Lunar Planet. Sci.* **21**, 57.

Bell, J. F., D. R. Davis, W. K. Hartmann, and M. J. Gaffey 1989a. The big picture. In *Asteroids II* (R. Binzel, T. Gehrels, and M. S. Matthews, Eds.), pp. 921–945. Univ. of Arizona Press, Tucson.

Bell, J. F., J. R. Piscitelli, and L. A. Lebofsky 1989b. Deimos: Hydration state from infrared spectroscopy. *Lunar Planet. Sci.* **20**, 58.

Bibring, J.-P., M. Combes, Y. Langevin, A. Soufflot, C. Cara, P. Drossart, T. Encrenaz, S. Erard, O. Forni, B. Gondet, L. Ksanfomality, E. Lellouch, P. Masson, V. Moroz, F. Rocard, J. Rosenqvist, and C. Sotin 1989. Results from the ISM experiment. *Nature* **341**, 591–593.

Boslough, M. B., R. J. Weldon, and T. J. Ahrens 1980. Release of water from hydrous minerals due to impact. *Lunar Planet. Sci.* **11**, 97–99.

Britt, D., J. F. Bell, H. Haack, and E. R. D. Scott 1992. The reflectance spectrum of troilite and the T-type asteroids. *Meteoritics Planet. Sci.* **27**, 207.

Burns, J. A. 1992. Contradictory clues as to the origin of the martian moons. In *Mars* (H. H. Kieffer, B. M. Jakosky, C. W. Snyder, and M. S. Matthews, Eds.), pp. 1283–1302. Univ. of Arizona Press, Tucson.

Bustani, D., J. F. Bell, J. Veverka, R. H. Brown, and D. P. Cruikshank 1997. Near-IR spectroscopy of Amalthea (JV) and Thebe (JXIV). *Bull. Am. Astron. Soc.* **29**, 1012.

Cantor, B. A., M. J. Wolff, P. C. Thomas, P. B. James, and G. Jensen 1999. Phobos disk-integrated photometry: 1994–1997 HST observations. *Icarus* **142**, 414–420.

Fanale, F. P., and J. R. Salvail 1989. Loss of water from Phobos. *Geophys. Res. Lett.* **16**, 287–290.

Fanale, F. P., and J. R. Salvail 1990. Evolution of the water regime of Phobos. *Icarus* **88**, 380–395.

Feierberg, M. A., L. A. Lebofsky, and D. Tholen 1985. The nature of C-class asteroids from 3- μ m spectrophotometry. *Icarus* **63**, 183–191.

Gaffey, M. J. 1976. Spectral reflectance characteristics of the meteorite classes. *J. Geophys. Res.* **81**, 905–920.

Gradie, J., and J. Veverka 1986. The wavelength dependence of phase coefficients. *Icarus* **66**, 455–467.

Gradie, J. C., C. R. Chapman, and E. F. Tedesco 1989. Distribution of taxonomic classes and the compositional structure of the asteroid belt. In *Asteroids II* (R. Binzel, T. Gehrels, and M. S. Matthews, Eds.), pp. 316–335. Univ. of Arizona Press, Tucson.

Grundy, W. M., and U. Fink 1992. Deimos: A reddish, D-type asteroid spectrum. In *Asteroids, Comets, Meteors 1991*, pp. 215–218. Lunar and Planetary Institute.

Hiroi, T., M. E. Zolensky, C. M. Pieters, and M. E. Lipschutz 1996. Thermal metamorphism of the C, G, B, and F asteroids seen from the 0.7 μ m, 3 μ m and UV absorption strengths in comparison with carbonaceous chondrites. *Meteoritics Planet. Sci.* **31**, 321–327.

Houk, N., and C. Swift (1999). *Michigan Catalogue of Two-Dimensional Spectral Types for the HD Stars*, Vol. 5. Univ. of Michigan, Ann Arbor.

Howell, E. S. 1995. *Probing Asteroid Composition Using Visible and Near-Infrared Spectroscopy*. Ph.D. dissertation, University of Arizona, Tucson.

Howell, E. S., A. S. Rivkin, R. P. Binzel, and S. J. Bus 1995. Spectral observations of the Mars Trojan 5261 Eureka. *Lunar Planet. Sci.* **26**, 633.

Jones, T. D., L. A. Lebofsky, J. S. Lewis, and M. S. Marley 1990. The composition and origin of the C, P, and D asteroids: Water as a tracer of thermal evolution in the outer belt. *Icarus* **88**, 172–192.

Ksanfomality, L., S. Murchie, D. Britt, T. Duxbury, P. Fisher, N. Goroshkova, J. Head, E. Kuhr, V. Moroz, B. Murray, G. Nikitin, E. Petrova, C. Pieters, A. Soufflot, A. Zharkov, and B. Zhukov 1991. Phobos-spectrophotometry between 0.3 and 0.6 micron and IR-radiometry. *Planet. Space Sci.* **39**, 311–326.

Lebofsky, L. A. 1980. Infrared reflectance spectra of asteroids: A search for water of hydration. *Astron. J.* **85**, 573–585.

Lebofsky, L. A., and J. R. Spencer 1989. Radiometry and thermal modeling of asteroids. In *Asteroids II*, (R. Binzel, T. Gehrels, and M. S. Matthews, Eds.), pp. 128–147. Univ. of Arizona Press, Tucson.

Lebofsky, L. A., T. D. Jones, P. D. Owensby, M. A. Feierberg, and G. J. Consolmagno 1990. The nature of low albedo asteroids from 3- μ m spectrophotometry. *Icarus* **83**, 12–26.

Lewis, J. S., D. S. McKay, and B. C. Clark 1993. Using resources from near-Earth space. In *Resources of Near-Earth Space* (J. S. Lewis, M. S. Matthews, and M. L. Guerrieri, Eds.), pp. 3–14. Univ. of Arizona Press, Tucson.

Lunine, J. I., G. Neugebauer, and B. M. Jakosky 1982. Infrared observations of Phobos and Deimos from Viking. *J. Geophys. Res.* **87**, 10297–10305.

- McCord, T. B., R. N. Clark, B. R. Hawke, L. A. McFadden, P. D. Owensby, C. M. Pieters, and J. B. Adams (1981). Moon—Near-infrared spectral reflectance, a first good look. *J. Geophys. Res.* **86**, 10883–10892.
- Merényi, E., E. S. Howell, A. S. Rivkin, and L. A. Lebofsky 1997. Prediction of water in asteroids from spectral data shortward of 3 μm . *Icarus* **129**, 421–439.
- Murchie, S., and S. Erard 1996. Spectral properties and heterogeneity of Phobos from measurements by Phobos 2. *Icarus* **123**, 63–86.
- Murchie, S. L., D. T. Britt, J. W. Head, S. F. Pratt, P. C. Fisher, B. S. Zhukov, A. A. Kuzmin, L. V. Ksanfomality, A. V. Zharkov, G. E. Nikitin, F. P. Fanale, D. L. Blaney, J. F. Bell III, and M. S. Robinson 1991. Color heterogeneity of the surface of Phobos—Relationships to geologic features and comparison to meteorite analogs. *J. Geophys. Res.* **96**, 5925–5945.
- Murchie, S., N. Thomas, D. Britt, K. Herkenhoff, and J. F. Bell III 1999. Mars pathfinder spectral measurements of Phobos and Deimos: Comparison with previous data. *J. Geophys. Res.* **104**, 9069–9080.
- Ostro, S. J., R. F. Jurgens, D. K. Yeomans, E. M. Standish, and W. Greiner 1989. Radar detection of Phobos. *Science* **243**, 1584–1586.
- Pang, K. D., J. B. Pollack, J. Veverka, A. L. Lane, and J. M. Ajello 1978. The composition of Phobos—Evidence for carbonaceous chondrite surface from spectral analysis. *Science* **199**, 64–66.
- Pieters, C. M. 1999. The Moon as a spectral calibration standard enabled by lunar samples: The Clementine example. In *Workshop on New Views of the Moon II: Understanding the Moon through the Integration of Diverse Datasets*, pp. 8025–8026. Lunar and Planetary Institute.
- Pollack, J. B., J. Veverka, K. D. Pang, D. S. Colburn, A. L. Lane, and J. M. Ajello 1978. Multicolor observations of Phobos with the Viking lander cameras—Evidence for a carbonaceous chondritic composition. *Science* **199**, 66–69.
- Rivkin, A. S., E. S. Howell, D. T. Britt, L. A. Lebofsky, M. C. Nolan, and D. D. Branton 1995. 3- μm spectrophotometric survey of M and E-class asteroids. *Icarus* **117**, 90–100.
- Rivkin, A. S., B. E. Clark, D. T. Britt, and L. A. Lebofsky 1997. Infrared spectrophotometry of the NEAR flyby target 253 Mathilde. *Icarus* **127**, 255–257.
- Rivkin, A. S., L. A. Lebofsky, B. E. Clark, E. S. Howell, and D. T. Britt 2000. The nature of M-class asteroids in the 3- μm region. *Icarus* **145**, 351–368.
- Roush, T. L., and R. C. Hogan 2000. Mars global surveyor thermal emission spectrometer observations of Phobos. *Lunar Planet. Sci.* **31**, Abstract 1598.
- Salisbury, J. W., D. M. D’Aria, and E. Jarosewich 1991. Midinfrared (2.5–13.5 μm) reflectance spectra of powdered stony meteorites. *Icarus* **92**, 280–297.
- Shure, M., D. W. Toomey, J. Rayner, A. Onaka, A. Denault, W. Stahlberger, D. Watanabe, K. Criez, L. Robertson, D. Cook, and M. Kidger 1994. A powerful new infrared array camera for the NASA infrared telescope facility. *Exp. Astron.* **3**, 239–242.
- Simonelli, D. P., P. C. Thomas, B. T. Carcich, and J. Veverka 1993. The generation and use of numerical shape models for irregular Solar System objects. *Icarus* **103**, 49–61.
- Simonelli, D. P., M. Wisz, A. Switala, D. Adinolfi, J. Veverka, P. C. Thomas, and P. Helfenstein 1998. Photometric properties of Phobos surface materials from Viking images. *Icarus* **131**, 52–77.
- Smith, D. E., F. C. Lemoine, and M. T. Zuber 1995. Simultaneous estimation of the masses of Mars, Phobos and Deimos using spacecraft distant encounters. *Geophys. Res. Lett.* **22**, 2171–2174.
- Spencer, J. R. 1990. A rough-surface thermophysical model for airless planets. *Icarus* **83**, 27–38.
- Tabachnik, S., and N. W. Evans 1999. Cartography for martian Trojans. *Astrophys. J.* **517**, L63–66.
- Tedesco, E. F., G. J. Veeder, J. W. Fowler, and J. R. Chillemi 1992. The IRAS Minor Planet Survey Data Base. National Space Science Data Center, Greenbelt, MD. (digital data).
- Thibault, C. A., M. E. Mickelson, and F. Vilas 1997. Reflectance spectroscopy of phyllosilicates from 0.4 to 1.0 μm . *Bull. Am. Astron. Soc.* **29**, Abstract 07.16.
- Thomas, P. C., D. Adinolfi, P. Helfenstein, D. Simonelli, and J. Veverka 1996. The surface of Deimos: Contribution of materials and processes to its unique appearance. *Icarus* **123**, 536–556.
- Tody, D. 1986. The IRAF data reduction and analysis system. In *Instrumentation in Astronomy VI* (D. L. Crawford, Ed.), Vol. 627, pp. 733. SPIE—Int. Soc. Opt. Eng., Bellingham, WA.
- Toomey, D. W., C. Ftaclas, R. H. Brown, and D. Trilling 1998. CoCo: An experiment in infrared coronagraphy at the IRTF. In *Infrared Astronomical Instrumentation* (A. M. Fowler, Ed.), Vol. 3354, pp. 782–790. SPIE—Int. Soc. Opt. Eng., Bellingham, WA.
- Veeder, G. J., D. L. Matson, and J. C. Smith 1978. Visual and infrared photometry of asteroids. *Astron. J.* **83**, 651–663.
- Veeder, G. J., D. L. Matson, E. F. Tedesco, L. A. Lebofsky, and J. C. Gradie 1987. Radiometry of Deimos. *Astron. J.* **94**, 1361–1363.
- Veverka, J., and P. Thomas 1979. Phobos and Deimos—A preview of what asteroids are like. In *Asteroids* (T. Gehrels, Ed.), pp. 628–651. Univ. of Arizona Press, Tucson.
- Veverka, J., J. F. Bell III, C. Chapman, M. Malin, L. A. McFadden, S. Murchie, M. Robinson, P. C. Thomas, D. K. Yeomans, A. Harch, B. G. Williams, B. Clark, R. W. Farquhar, A. Cheng, and D. W. Dunham 1997. NEAR’s flyby of mainbelt Asteroid 253 Mathilde. *Bull. Am. Astron. Soc.* **29**, 958.
- Wang, S.-I., P. D. Owensby, D. W. Toomey, R. H. Brown, W. E. Stahlberger, C. P. Cavedoni, R. Hua, and C. Ftaclas 1994. CoCo: An infrared cold coronagraph for astronomical observations. In *Instrumentation in Astronomy VIII* (D. L. Crawford and E. R. Craine, Eds.), Vol. 2198, pp. 578–589. SPIE—Int. Soc. Opt. Eng., Bellingham, WA.
- Zellner, B., D. J. Tholen, and E. F. Tedesco 1985. The eight-color asteroid survey: Results for 589 minor planets. *Icarus* **61**, 355–416.